Archives of Mechanics • Archiwum Mechaniki Stosowanej • 30, 2, pp. 123-133, Warszawa 1978

Oxygen dissociation relaxation behind oblique reflected and stationary oblique shocks

H. OERTEL jr. (KARLSRUHE)

OXYGEN dissociation relaxation has been calculated and measured behind regular reflected and stationary oblique shocks. Numerical calculations informed about the possible experimental conditions and the relaxation zone data. Photographs of the shock configuration have been taken and density profiles of the relaxation zones have been measured by means of a multi-beam-laser-differentialinterferometer. The measured density profiles clearly revealed the need for revising oxygen dissociation rates. New reaction rate coefficients have been determined using numerical fitting.

Przeprowadzono pomiary i obliczenia relaksacji dysocjacji tlenu za frontem regularnej odbitej i stacjonarnej, skośnie padającej fali uderzeniowej. Wykonano obliczenia numeryczne w celu przybliżonego określenia warunków doświadczalnych oraz danych dla obszarów relaksacji. Uzyskano fotografie konfiguracji fal uderzeniowych oraz zmierzono profile gęstości oraz obszary relaksacji za pomocą wielowiązkowego, różniczkowego, laserowego interferometru. Zmierzone profile gęstości wskazały w sposób oczywisty na potrzebę zrewidowania praw dysocjacji tlenu. Określono nowe współczynniki prędkości reakcji przez odpowiednie dopasowanie wyników numerycznych.

Проведены измерения и расчеты релаксации диссоциации кислорода за фронтом регулярной, отраженной и стационарной, косо падающей ударной волной. Проделаны численные расчеты с целью приближенного определения экспериментальных условий и данных для областей релаксации. Получены фотографии конфигураций ударных волн, измерены профили плотности и области релаксации при помощи многолучевого, лазерного интерферометра. Измеренные профили плотности указали очевидным образом на необходимость пересмотра законов диссоциации кислорода. Определены новые коэффициенты скорости реакции путем соответствующего подбора численных результатов.

1. Introduction

OXYGEN dissociation has been extensively studied in shock tubes behind normal shocks, bow waves ahead of different models, with nozzle flows as well as within expansions following shock compression. The results have been compiled and discussed in several books and reviewing reports. Having compared calculated relaxation zones behind incident, regular reflected and stationary oblique shocks, we concluded that the investigation of dissociation relaxation behind oblique shocks offers some important advantages: the temperature variation during relaxation can be varied by simply changing the wedge angle. High degrees of dissociation can be obtained in a simple shock tube without heating the driver gas. The experimental conditions can be choosen such that the oxygen has high translation temperature or is partly dissociated ahead of the shock. This offers the possibility of investigating oxygen dissociation relaxation in a new way. On the other side there was some doubt as to whether these obvious advantages could be realized in the shock

tube at our disposal. Combined molecular transport and relaxation effects near the wall of the wedge could perhaps not be neglected. The oblique shocks could perhaps not become stationary. These problems were the first to be investigated theoretically and experimentally. Numerical calculation preparing experiments as well as recalculations evaluating experi-

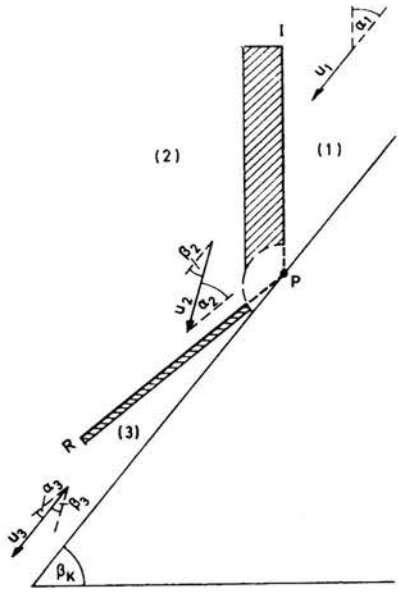

FIG. 1. Sketch of regular shock reflection.

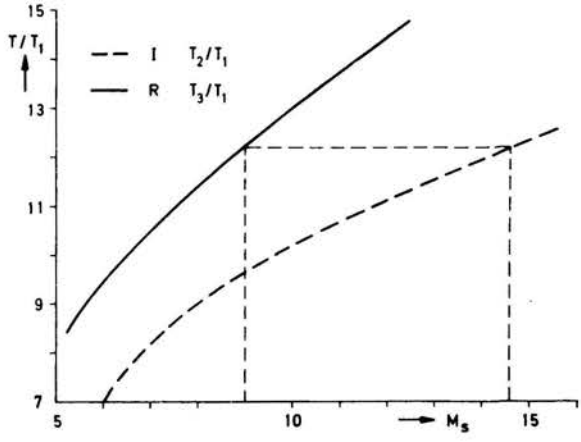

FIG. 2. Temperature behind the incident and reflected shock, $p_1 = 1$ Torr, $T_1 = 293$ K, $\beta_K = 60°$.

ments have been done. Photographs of the shock configuration have been taken and density profiles of the relaxation zones have been measured by means of a multi-beam-laser-differentialintereferometer.

2. Calculations

2.1. Regular shock reflection

Regular shock configuration was assumed to be stationary in the moving frame of the reflection point P as shown in Fig. 1. The gas coming from the thermodynamic equilibrium state (1), goes to the equilibrium state (2) behind the incident shock I and then to the equilibrium state (3) behind the reflected shock R passing through the shadowed relaxation zones. The flow velocity behind the reflected shock is adopted to be parallel to the wall. We completely neglected the overlapping region of the relaxation zones of the incident and reflected shock as well as boundary layer effects. We also neglected viscosity, diffusion and heat conduction within the relaxation zones far from the wall.

Within the dissociation relaxation zones two reaction pairs have been considered:

$O_2 + O_2 \overset{1}{\rightleftharpoons} 2O + O_2$	$\overrightarrow{k_1} = A_1 T^{B_1} \exp\left(-\frac{\Theta_D}{T}\right)$
$O_2 + O \overset{2}{\rightleftharpoons} 3O$	$\overrightarrow{k_2} = A_2 T^{B_2} \exp\left(-\frac{\Theta_D}{T}\right)$

with dissociation rates $\overrightarrow{k_1}$ and $\overrightarrow{k_2}$. For the calculations the values of Chapter 4 have been used.

The numerical results revealed some possible advantages of investigating relaxation behind regular reflected shocks. Figure 2 shows that the equilibrium temperature behind the reflected shock amounts to 3560 K at incident shock Mach number 9. Producing the same equilibrium temperature behind the incident shock requires a shock Mach number as high as 14.6, which can only be obtained with heated driver gas. An even more important advantage is that the temperature variation during relaxation is smaller than that encounter-

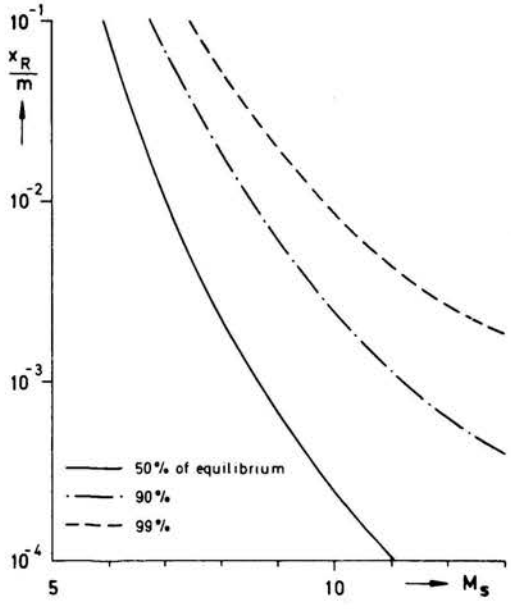

FIG. 3. Dissociation relaxation zone length x_R, $p^1 = 1$ Torr, $\beta_K = 60°$, $T_1 = 293$ K.

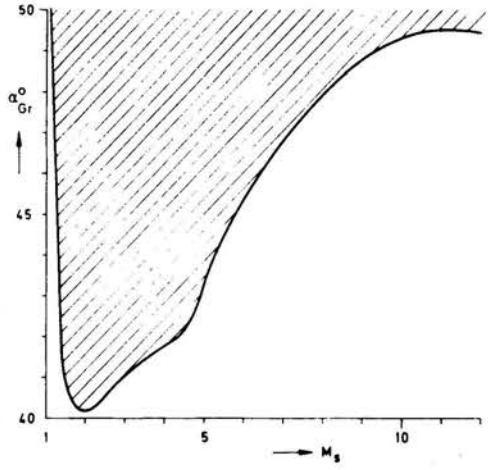

FIG. 4. Critical incidence angle α_{Gr}, $p_1 = 1$ Torr, $T_1 = 293$ K.

ed at equal equilibrium temperature behind the incident shock. For instance, in the case of 3560 K the temperature variation during dissociation relaxation amounts to 5000 K behind the incident shock, to be compared with only 2000 K behind the reflected shock. High temperature variations within the relaxation zone have been one of the main sources of error when determining rate coefficients.

In Fig. 3 the 50%, 90% and 99% lengths of the dissociation relaxation zones behind the reflected shocks are plotted as a function of the shock Mach number M_S. For instance,

the dissociation relaxation zone has a 90% length of 6 mm at $M_S = 9$. Relaxation zone length has been defined as the normal distance at which the relaxation variable has reached 90% of its equilibrium value.

Calculating the ratio of relaxation zone lengths behind the incident and reflected shock we recognized the ratio 100 of the dissociation relaxation lengths at the shock Mach number $M_S = 9$. This means that quite a large range of conditions may exist where the reflected shock runs into the frozen state behind the incident shock, frozen with respect to dissociation. The evaluation of experimental density profiles has to be done with this assumption.

In Fig. 4 the critical incidence angle α_{Gr} is plotted as a function of the incident shock Mach number M_S. Only at angles smaller than α_{Gr} regular shock reflection exists. At incidence angles larger than α_{Gr}, in the shadowed area, Mach reflection occurs. This diagram reveals an important limitation of possible experimental conditions.

2.2. Stationary oblique shock

The adopted shock configuration is shown in Fig. 5. The gas enters into the oblique shock S having a shock angle α_2 with a flow velocity u_2 and thermodynamic equilibrium state (2). After having passed through the shadowed relaxation zone it comes to the equilibrium state (3) and flow velocity u_3 which is assumed to be parallel to the wall. β_K denotes

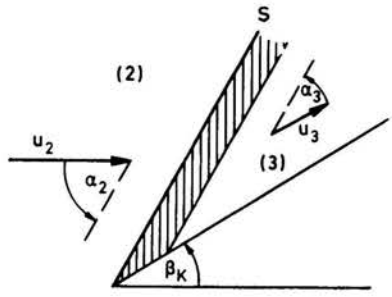

FIG. 5. Sketch of the stationary oblique shock.

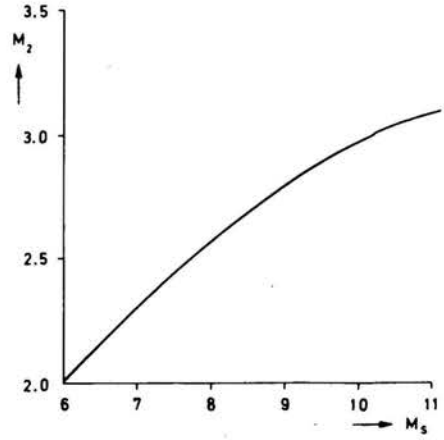

FIG. 6. Shock Mach number M_2, $p_1 = 1$ Torr, $T_1 = 293$ K.

the wedge angle. The equilibrium state (2) ahead of the oblique shock S is produced by the incident shock running with the shock Mach number M_S into state (1). The shock Mach number M_2 in state (2) is plotted in Fig. 6 as a function of M_S.

In Fig. 7 the critical wedge angle is plotted as a function of the incident shock Mach number M_S. At wedge angles larger than $\beta_{K_{max}}$ the detached bow wave occurs. For wedge angles smaller than $\beta_{K_{min}}$ we calculated fully dispersed shocks. Only in the area not shadowed the assumptions of our theoretical model are met.

Figure 8 shows the 50%, 90% and 99% dissociation relaxation zone lengths. For instance, the dissociation relaxation zone has a 90% length of 1.6 cm at the shock Mach number 10.

Another important theoretical result was that the shock tube test time is not too short for reaching the thermodynamic equilibrium state (2) ahead of the oblique shock. For

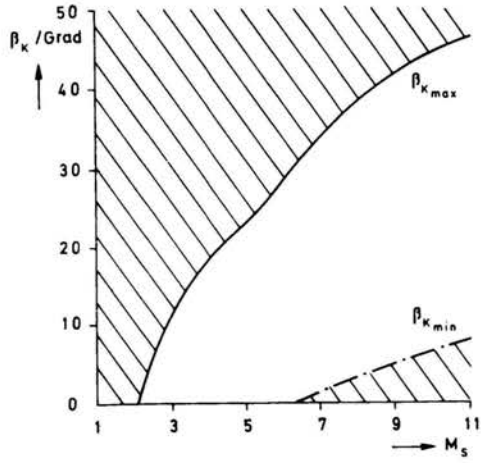

FIG. 7. Critical wedge angle $\beta_{K\max}$, $\beta_{K\min}$, $p_1 = 1$ Torr, $T_1 = 293$ K.

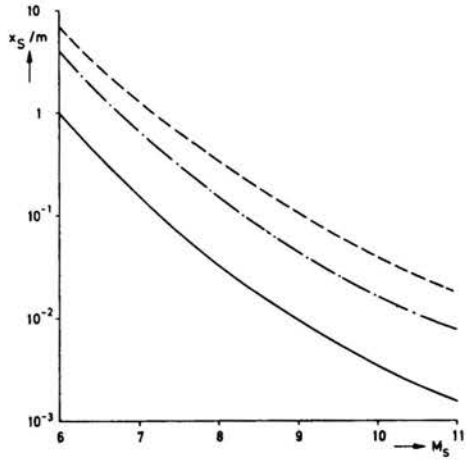

FIG. 8. Dissociation relaxation zone length x_S, $p_1 = 1$ Torr, $T_1 = 293$ K, $\beta_K = 30°$.

instance, at the shock Mach number $M_S = 9.5$ and initial pressure $p_1 = 1$ Torr we reach 12% degree of dissociation ahead of the oblique shock, and the equilibrium temperature amounts to 2930 K. This means that in a wide range of experimental conditions the advantageous investigation of dissociation relaxation in partly dissociated oxygen is possible.

Experiments had to confirm that the adopted theoretical model is adequate.

3. Experiments

3.1. Facility

The University of Karlsruhe — low pressure shock tube was used, which has a 12.5 m total length and a 15 cm diameter. Hydrogen at initial pressure 1 bar to 10 bar served as driver gas. The test gas was high purity oxygen with initial pressures 1 Torr to 3 Torr. The highest shock Mach number obtained was $M_S = 9.5$. A part of the shock wave penetrated into a 9 cm $\times$ 9 cm rectangular cross-section tube. The wedge was fixed between 11 cm diameter windows.

3.2. Shock configurations

Shock configurations at different wedge angles were visualized by complementary double exposure interferography described by Smeets, George and Oertel jr. The optical set up of the differential interferometer is sketched in Fig. 9. The double exposure with

opposite circular polarised light of two spark light sources compensates optical faults which otherwise would distort the quality of the pictures at the infinite fringe spacing needed for visualizing the low density flow.

Figure 10 presents one typical interferogram of the regular shock reflection at the incident shock Mach number $M_S = 9.2$. The interferogram clearly shows that the reflected

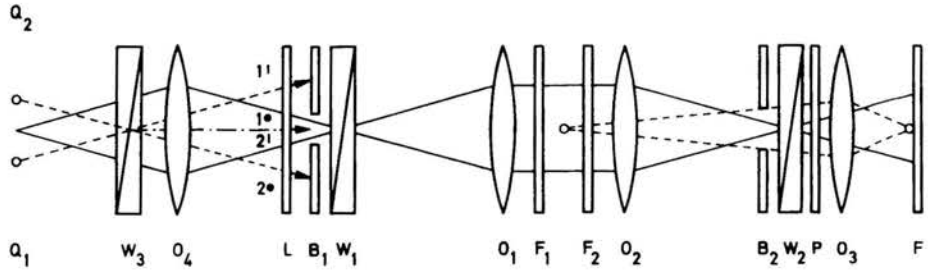

FIG. 9. Double exposure of differentialinterferometer.

FIG. 10. Regular shock reflection,
$M_S = 9.2$, $\beta_K = 70°$, $p_1 = 1$ Torr, $T_1 = 295$ K.

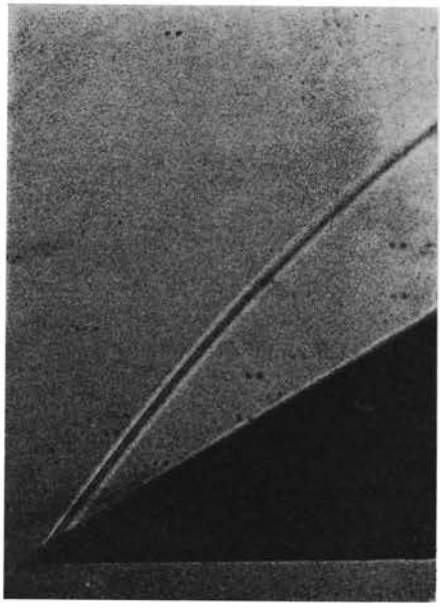

FIG. 11. Stationary oblique shock,
$M_S = 9.3$, $\beta_K = 30°$, $h_1 = 1$ Torr, $T_1 = 298$ K.

shock is straight in spite of the relaxation and the transport phenomena in the wall boundary layer. Many of such interferograms confirmed this fact and supported the basic assumption of our theoretical model.

Figure 11 shows one interferogram of the stationary oblique shock at the incident shock Mach number 9.3. The oblique shock is straight near the edge of the wedge. This means that the density variations within relaxation are so weak that they don't curve the shock near the edge of the wedge. Many of such interferograms confirmed this fact. The

experimental reflection angles α_3 and shock angles α_2 taken from such pictures have been found to be 10% to 15% larger than those calculated with the hypotheses of wall parallel equilibrium flow. This may be due to the combined viscous and entropy layer displacement effect. We concluded that we have to evaluate our measured density profiles with the measured reflection angles and shock angles and not with the calculated ones.

3.3. Density profiles

The density profiles of the relaxation zones behind the incident, reflected and stationary oblique shocks were measured by means of laser-differentialinterferometers as described by Smeets, George and Oertel jr. Two of these are sketched in Fig. 12. The optical set up is similar to that of Fig. 9. A 15 mW He-Ne-laser was used as the light source. PIN-diodes served as detectors and the signals were stored by means of oscilloscopes. The laser-differentialinterferometers have a space resolution of 0.2 mm and a time resolution of 0.1 μ s. In the case of regular shock reflection we used four interferometers as shown in Fig. 13.

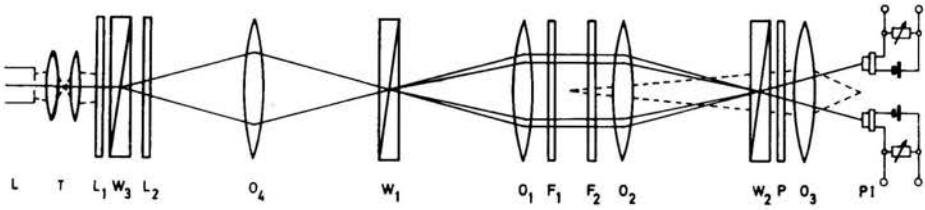

FIG. 12. Laser-differentialinterferometer.

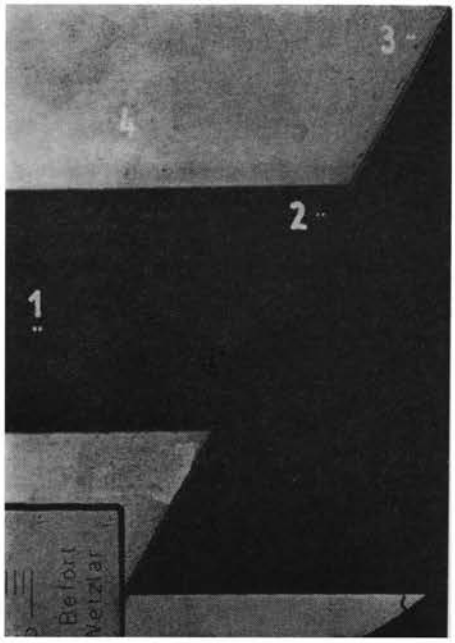

FIG. 13. Arrangement of laser-differentialinterferometers, regular shock reflection.

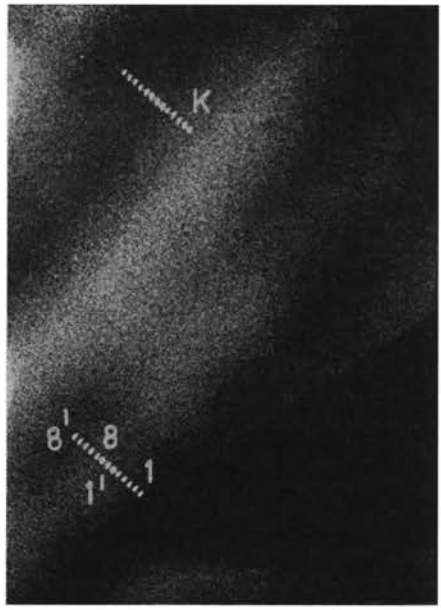

FIG. 14. Arrangement of laser-differentialinterferometers, stationary oblique shock.

The use of four interferometers offered the possibility of measuring simultaneously the speed of the incident shock, the reflection angle α_3 and two density profiles of the relaxation zone behind the reflected shock at each experiment. In this way it was found that the regular shock reflection is stationary in the moving frame and that the relaxation zones are one-dimensional. The details of the signal evaluation have been described by Oertel jr. The results of the measured density profiles are presented and the evaluation of the dissociation rates is explained in the next chapter.

To measure dissociation relaxation zones behind stationary oblique shocks eight laser-differentialinterferometers have been used simultaneously. The arrangement is shown in Fig. 14; 1′–8′ denote the reference beams. One interferometer K located in the equilibrium state (2) ahead of the oblique shock was used to compensate mechanical vibrations.

4. Recalculations evaluating experiments

We calculated the relaxation zones with different published reaction rate coefficients $\overrightarrow{k_1}$ and $\overrightarrow{k_2}$ using measured reflection angles α_3 and measured shock angles α_2 and not the theoretical boundary conditions. We compared these with the experimental ones. There

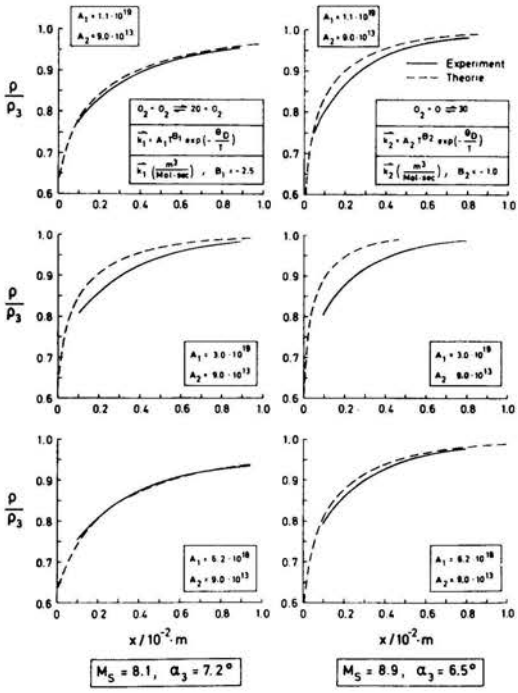

FIG. 15. Fitting procedure. Dissociation relaxation zone density profiles behind reflected shocks,
——— theory, — — — — — experiment,
$p_1 = 1$ Torr $T_1 = 295$ K.

was no set of dissociation rates that described sufficiently well our experimental results at all experimental conditions. We concluded that a new redetermination of the oxygen dissociation rates was needed using numerical fitting.

The applied fitting procedure was the following one:

The experimental density profiles were approximated by a sum of exponential functions with a last-squares-fit giving deviations not exeeding 1‰. For all experimental conditions we then calculated the theoretical profiles inserting varied constants A_1 and A_2 for different sets of B_1 and B_2. The fit was considered to be successful if for all experimental conditions

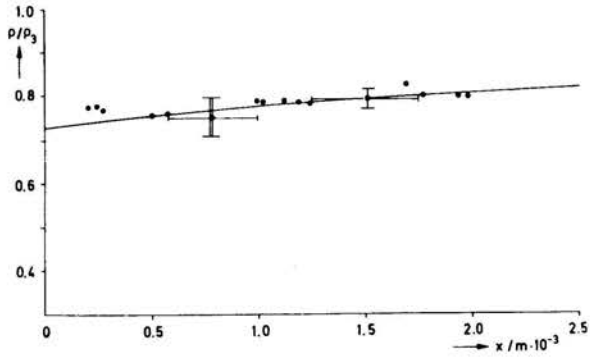

FIG. 16. Dissociation relaxation zone density profile behind the stationary oblique shock

experiment, ——— theory,

$M_S = 9.5$, $p_1 = 1$ Torr, $\beta_K = 30°$, $\alpha_2 = 50°$.

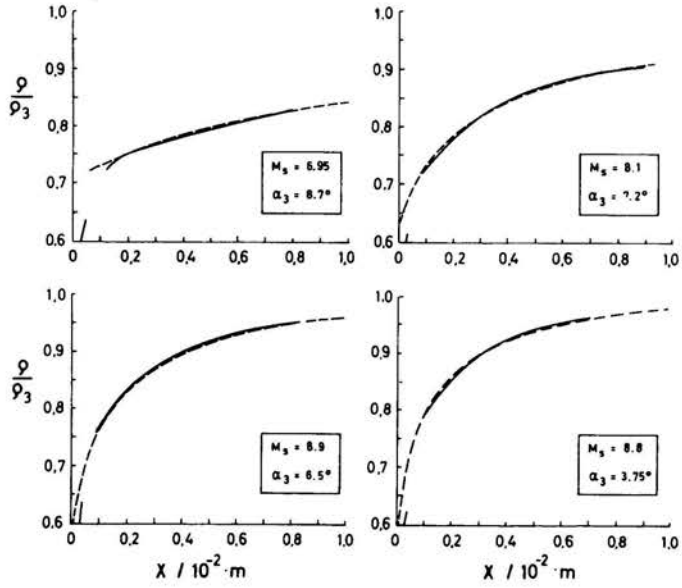

FIG. 17. Dissociation relaxation zone density profiles behind the reflected shock, ——— theory, ——————— experiment, $p_1 = 1$ Torr, $T_1 = 295$ K.

the last-squares-deviation between the measured and calculated profiles was less than the experimental error.

Three examples of the fitting procedure for two different experimental conditions of regular shock reflection are shown in Fig. 15. The ratio of density ϱ and equilibrium density ϱ_3 is plotted as a function of the normal shock distance x. The experimental and theoretical density profiles, calculated with varied dissociation rates, do not agree as yet for the two considered experimental conditions.

The result of the numerical fit is shown in Figs. 16 and 17 for five examples.

It can be seen now that the experimental and the new theoretical dissociation relaxation zone density profiles agree very well for the regular shock reflection as well as for the stationary oblique shock. Some discrepancy at the beginning of the relaxation zones behind the reflected shock is due to vibrational relaxation. We assumed a frozen state at the beginning of the relaxation zone with molecular translation, rotation and vibration in equilibrium and dissociation frozen. Therefore the density profile at the beginning cannot be compatible with our theoretical model. This part of the experimental profile was excluded from fitting.

Also all other profiles measured at 20 different experimental conditions agreed as well with the theoretical ones which we recalculated with the new dissociation rates.

The final result of the evaluation of the oxygen dissociation rates in the temperature range 3100 K to 7000 K is the following one:

$O_2+O_2 \rightleftharpoons 2O+O_2$	$\overrightarrow{k_1} = A_1 T^{-2.5} \exp\left(-\frac{\Theta_D}{T}\right)$
$O_2+O \rightleftharpoons 3O$	$\overrightarrow{k_2} = A_2 T^{-1.0} \exp\left(-\frac{\Theta_D}{T}\right)$

$$A_1 = (6.2 \pm 0.5)\,10^{18}\,\frac{\mathrm{m}^3}{\mathrm{mol}\cdot\mathrm{sec}}, \quad A_2 = (4.0 \mp 0.5)\,10^{13}\,\frac{\mathrm{m}^3}{\mathrm{mol}\cdot\mathrm{sec}}$$

The indicated deviation ± 0.5 results from experimental errors. Within this range positive deviation of $\overrightarrow{k_1}$ can be compensated by a negative one of $\overrightarrow{k_2}$.

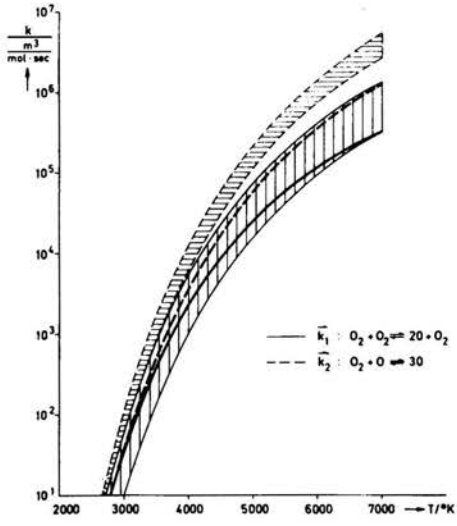

FIG. 18. Oxygen dissociation rate coefficients.

The values of the new dissociation rate coefficients are now to be compared with those previously published by other authors. Figure 18 presents the result by means of a plot of the dissociation rates $\overrightarrow{k_1}$ and $\overrightarrow{k_2}$ as functions of the temperature T. The published values of Bortner, Byron, Camac, Hall, Mathews, Martins and Wray are within the shadowed

areas. The thick lines represent the new dissociation rate coefficients. The dissociation rate $\overrightarrow{k_1}$ remains within the shadowed area but comes to its lower limit at high temperatures. The new dissociation rates $\overrightarrow{k_2}$ are significantly smaller than what was assumed up to date.

5. Conclusions

Measuring dissociation relaxation density profiles behind regular reflected and stationary oblique shocks by means of laser-differentialinterferometers has been proved to be a good method. The theoretical model used for the numerical calculations was confirmed by experiments. Especially the photographs revealed the regular reflected shocks to be straight near the reflection point and the stationary oblique shocks near the edge of the wedge. To understand this phenomenon in all details further theoretical and experimental investigations are necessary. The described method could be applied to gases other than oxygen.

The results obtained can be used for more precise calculations of dissociation relaxation effects on flows of hot gases containing oxygen. The calculations of regular shock reflection and stationary oblique shocks with and without relaxation have shown that these effects are quite strong.

Acknowledgments

The author wishes to express his appreciation to Prof. Dr B. SCHMIDT and Prof. Dr. J. ZIEREP for valuable suggestions and stimulating discussions during the investigations. The work was supported by the Gesellschaft für Weltraumforschung and Deutsche Forschungsgemeinschaft. All numerical calculations were performed with the aid of the Univac 1108 of the Rechenzentrum der Universität Karlsruhe.

References

1. K. BERNZOTT, B. SCHMIDT, H. OERTEL jr., Appl. Phys., 11, 281–284, 1976.
2. M. H. BORTNER, A. GOLDEN, General Elect., 61 SDO 23 Me 440, 1961.
3. S. R. BYRON, J. Chem. Phys., **30**, 6, 1959.
4. M. CAMAC, R. M. FEINBERG, The Comb. Inst., Pa. 137–145, Pittsburgh 1967.
5. J. G. HALL, A. L. RUSSO, Agard Conf. Proc., 12, 443, 1967.
6. J. J. MARTIN, *Atmospheric Reentry*, Prentice Hall, N. J., 1966.
7. D. L. MATHEWS, Physics of Fluids, 2, 170, 1959.
8. H. OERTEL jr., Dissertation, Karlsruhe 1974.
9. H. OERTEL jr., J. F. M., 74, 477, 1976.
10. B. SCHMIDT, H. OERTEL jr., BMFT-Bericht W 75–16, 1975.
11. G. SMEETS, A. GEORGE, ISL-Bericht 39/72, 1972.
12. G. SMEETS, A. GEORGE, ISL-Bericht 14/71, 1971.
13. K. L. WRAY, J. Chem. Phys., 38, 1518, 1963.

INSTITUT FÜR STRÖMUNGSLEHRE UND STRÖMUNGSMASCHINEN
UNIVERSITÄT KARLSRUHE, GFR.

Received September 16, 1975.